Paper resubmitted to the International Journal of Fracture, March 2000. (Revised August 2000)

Mixed Mode Cracks in Reissner Plates

R. K. L. Su[a,1]
Ph.D. Assistant Professor

A. Y. T. Leung[b]
D.Sc., Ph.D. Professor, Head of Department

[a] Department of Civil Engineering, University of Hong Kong, Pokfulam Road, Hong Kong
[b] Department of Building and Construction Engineering, City University of Hong Kong, Tat Chee Avenue, Hong Kong
[1] Corresponding Author: Fax (852) 2559 5337

Total Number of Pages: 36

Number of Tables: 2

Number of Figures: 8

Abstract- Based on the sixth order Reissner plate theory, the generalized displacement functions for a cracked plate are derived by eigenfunction expansion method. The fractal two-level finite element method is employed to obtain the stress (moment and shear) intensity factors for the center cracked plate subjected to out-of-plane bending and twisting loads. The numerical results from the present method are checked with those available in literature. Highly accurate stress intensity factors are predicted for a wide range of thickness to crack length ratio and a full range of Poisson's ratio provided that the radius of fractal mesh to thickness ratio is not less than 1/10.

1. Introduction

When plates containing through thickness cracks and subjected to general loadings, the important crack parameters: stress intensity factors and moment intensity factors should be determined accurately in order to predict failure. Sih *et al*. [1] using the fourth order classical plate theory determined the stress intensity factors of crack tips for plane extensions and plate bendings. The Kirchhoff theory was employed such that the three physically distinct boundary conditions on the crack surface were reduced to two approximate boundary conditions. Thus the solutions obtained by Sih are not physically realistic. To improve the accuracy, a sixth or higher order theory such as Reissner/Mindlin plate theory was proposed to solve the cracked plate problems. It was first considered by Knowles and Wang[2] using singular integral equations with a Cauchy type kernel and the Reissner plate theory to derive an approximate numerical solution for crack in a vanishingly thin plate subject to pure bending. Hartranft *et al*.[3] and Wang[4] used dual integral equation techniques to extend independently the solutions to cracked finite thickness plate. Wang[5] employed the dual integral equations and variational procedure to further extend the numerical solutions for cracks of thick plate subjected to pure twisting. Joseph and Erdogan[6] queried the validly of the solutions [2] and [3] when close to the crack tips. They used perturbation methods and collocation techniques to solve the integral equations of cracked Reissner plates and obtained an extremely precise numerical solution for the bending stress intensity factors. This stress intensity factor was found not to be conversed to the thin plate limit $\frac{1+\nu}{3+\nu}$ as reported by Hartranft *et al*.[3]. Recently, Young and Sun[7] made use of both classical and Reissner/Mindlin plate theories to calculate the total strain energy release rate of cracked plates subjected to out-of-plane tearing loads. They found that the total strain energy release rate according to Reissner plate theory converges to that of classical plate theory as the

thickness to crack length ratio approaches zero. Subsequently, Hui and Zehnder[8] using J-integral techniques derived a universal relationship between the Kirchhoff theory stress intensity factors and the Reissner theory stress intensity factors for thin plates. They found that at the thin plate limit, the mode I moment intensity factor based on Reissner theory would converse to $\sqrt{\frac{1+\nu}{3+\nu}}$ which is agreed with the precise analytical results [6]. In spite of the significant achievements of the above-mentioned analytical studies for the cracked plates, nearly all the studies were limited to cracks in infinite plates. Only a few analytical studies attempted to solve the problems of cracks in finite plates. Examples are Murthy et al. [9] and Boduroglu et al. [10].

Since 1970, alternative formulations, mainly numerical ones have been developed rapidly based on higher order theories to solve the pertinent problem such as [11-20]. Among all the references, only reference [16] really solved the mode I, mode II and mode III problems, all the others dealt with mode I problem only. Thus the reliability of their proposed methods on mode II and mode III problems, which are commonly encountered during the practical situations, are questionable and pose serious uncertainties to the engineering designs. It is important to note that those numerical studies [11,12 and 17] claimed to be accurate for the thin plate limit are in fact agreed with the analytical results by Hartranft *et al*.[3] which were recently proved to be inaccurate by Joseph and Erdogan [6]. Moreover, it has been reported that the accuracy of some of the mentioned methods [18 and 19] fails when approaching the case of a thin plate. It is therefore important to seek a solution procedure that is highly accurate and consistent for all the modes and for the wide range of plate thickness.

Recently, the fractal two-level finite element method (F2LFEM) [20-24] was developed to tackle problems of cracked plates subject to bending and stretching loads. The objective of the present paper is to extend the F2LFEM to solutions of Reissner plate with a crack subjected to bending and twisting loadings. The accurate of the calculated stress intensity factors would be checked against wide range of thickness to crack length ratio and full range of Poisson's ratio. We suggested that while the interpolating shape functions within a finite element reduce the infinite number of degrees of freedom of a continuum to a finite number of degrees of freedom associated with the nodal displacements, global interpolating functions for the nodal displacements can also reduce the number of unknowns to a large extent. The global interpolating functions can be obtained by eigenfunction expansion technique based on Reissner plate theory. The fractal transformation method is introduced so that infinite number of finite elements and the associated infinitely many degrees of freedom are transformed in an expeditious way.

It is worthwhile to mention that the crack closure effect for mode I problems generally reduces the stress intensity factors by 10-45% (refers to Murthy et al.[25], Joseph and Erdogan [26] and Young and Sun [27]). Therefore, the effect of crack closure is conveniently and conservatively neglected in the present study. For practical engineering designs where the presence of slightly tensile loading may reduce the influence of closure effect, it may also be safer to neglect this beneficial effect.

2. Global Interpolating Functions

2.1. Eigenfunction expansion method for cracked plate

The use of Eigenfunction expansions in the Reissner theory for plate to evaluate the asymptotic behavior of relevant field quantities was first suggested by Sosa[28]. The leading

coefficients of up to the fourth term were derived. Using the similar procedure, leading coefficients of up to the eighth term are determined and presented in the following sections.

With reference to a rectangular coordinate system (x_1, x_2, x_3), a plate is considered here as an elastic body bounded by two parallel plates $x_3 = \pm h/2$. According to Reissner plate theory, three main assumptions are made:

i) displacements are small compared to the plate thickness,

ii) the stress normal to the midsurface of the plate is negligible,

iii) normals to the midsurface before deformation remain straight but not necessarily normal to the midsurface after deformation.

For a typical Reissner plate, the plate displacement vector **u** is expressed as,

$$\mathbf{u} = \begin{pmatrix} \psi_1 \\ \psi_2 \\ w \end{pmatrix} \tag{1}$$

in which w is the lateral plate displacement normal to x_1-x_2 plane and variables ψ_1 and ψ_2 are the normal rotations in x_1-x_3 and x_2-x_3 planes respectively. The sign conventions for plate displacements and plate forces for Reissner plate are depicted in Figure 1.

INSERT FIGURE 1 AROUND HERE

As in any crack problem, it is essential to choose an appropriate coordinate system. Assuming the crack lines along the -x_1 axis, it is suitable to use the polar coordinates r and θ, located at the crack tip. By using the linear theory of elasticity, the equilibrium equations could be written as,

$$\frac{\partial M_{rr}}{\partial r} + \frac{\partial M_{r\theta}}{r\partial \theta} + \frac{M_{rr} - M_{\theta\theta}}{r} - Q_r = 0, \tag{2}$$

$$\frac{\partial M_{r\theta}}{\partial r}+\frac{\partial M_{\theta\theta}}{r\partial\theta}+\frac{2}{r}M_{r\theta}-Q_{\theta}=0, \tag{3}$$

and $$\frac{\partial Q_r}{\partial r}+\frac{\partial Q_{\theta}}{r\partial\theta}+\frac{Q_r}{r}=0. \tag{4}$$

Also the moment and shear forces expressed in terms of the plate displacements were given by

$$M_{rr}=D\left[\frac{\partial\psi_r}{\partial r}+\frac{\nu}{r}\left(\psi_r+\frac{\partial\psi_{\theta}}{\partial\theta}\right)\right], \tag{5}$$

$$M_{\theta\theta}=D\left(\frac{\psi_r}{r}+\frac{\partial\psi_{\theta}}{r\partial\theta}+\nu\frac{\partial\psi_r}{\partial r}\right), \tag{6}$$

$$M_{r\theta}=D\frac{1-\nu}{2}\left(\frac{\partial\psi_{\theta}}{\partial r}+\frac{\partial\psi_r}{r\partial\theta}-\frac{\psi_{\theta}}{r}\right), \tag{7}$$

$$Q_r=D\frac{5(1-\nu)}{h^2}\left(\frac{\partial w}{\partial r}+\psi_r\right), \tag{8}$$

$$Q_{\theta}=D\frac{5(1-\nu)}{h^2}\left(\frac{\partial w}{r\partial\theta}+\psi_{\theta}\right), \tag{9}$$

in which $D=\dfrac{Eh^3}{12(1-\nu^2)}$ is the flexural rigidity and E is the Young's modulus. By substituting the plate forces (5-9) into the equilibrium equations (2-4), one can obtain the Navier equations for Reissner plate,

$$\begin{aligned}&-2\left[h^2+5r^2(1-\nu)\right]\psi_r-h^2(3-\nu)\frac{\partial\psi_{\theta}}{\partial\theta}+h^2(1-\nu)\frac{\partial^2\psi_r}{\partial\theta^2}+2h^2r\frac{\partial\psi_r}{\partial r}\\&\quad-10r^2(1-\nu)\frac{\partial w}{\partial r}+h^2r(1+\nu)\frac{\partial^2\psi_{\theta}}{\partial r\partial\theta}+2h^2r^2\frac{\partial^2\psi_r}{\partial r^2}=0\end{aligned}, \tag{10}$$

$$\begin{aligned}&-\left(h^2+10r^2\right)(1-\nu)\psi_{\theta}+h^2(3-\nu)\frac{\partial\psi_r}{\partial\theta}-10r(1-\nu)\frac{\partial w}{\partial\theta}+2h^2\frac{\partial^2\psi_{\theta}}{\partial\theta^2}\\&+h^2r(1-\nu)\frac{\partial\psi_{\theta}}{\partial r}+h^2r(1+\nu)\frac{\partial^2\psi_r}{\partial r\partial\theta}+h^2r^2(1-\nu)\frac{\partial^2\psi_{\theta}}{\partial r^2}=0\end{aligned}, \tag{11}$$

$$\frac{\partial^2 w}{\partial \theta^2} + r\left(\psi_r + \frac{\partial \psi_\theta}{\partial \theta} + \frac{\partial w}{\partial r}\right) + r^2\left(\frac{\partial \psi_r}{\partial r} + \frac{\partial^2 w}{\partial r^2}\right) = 0. \tag{12}$$

Further introducing the traction-free boundary conditions at the crack faces, we get

$$M_{\theta\theta} = M_{r\theta} = Q_\theta = 0 \quad \text{for} \quad \theta = \pm\pi\,. \tag{13}$$

The solutions of the Navier equations are conveniently represented as the double infinite series

$$D(1-\nu)\psi_r = \sum_{m=0}^{\infty}\sum_{n=0}^{\infty} r^{\lambda_m+n} U_n\,, \tag{14}$$

$$D(1-\nu)\psi_\theta = \sum_{m=0}^{\infty}\sum_{n=0}^{\infty} r^{\lambda_m+n} V_n\,, \tag{15}$$

$$D(1-\nu)w = \sum_{m=0}^{\infty}\sum_{n=0}^{\infty} r^{\lambda_m+n} W_n\,, \tag{16}$$

where U_n, V_n and W_n are functions of θ. After substituting the series into the Navier equations and considering the boundary conditions (13), the solution of the eigenvalue problem gives,

$$\lambda_m = \pm\frac{m}{2}, \quad m = 0,1,2,\cdots. \tag{17}$$

All the negative values of λ_m are rejected due to the results of unacceptable stresses and displacements. Then the double series (14-16) are simplified to the single series such that

$$D(1-\nu)\psi_r = \sum_{n=0}^{\infty} r^{n/2} f_n \tag{18}$$

$$D(1-\nu)\psi_\theta = \sum_{n=0}^{\infty} r^{n/2} g_n \tag{19}$$

$$D(1-\nu)w = \sum_{n=0}^{\infty} r^{n/2} h_n \tag{20}$$

where f_n, g_n and h_n are the eigenfunctions with variables of θ and ν only. Substituting equations (18-20) into the Navier equations (10-12) and the force and moment resultant equations (6-9) we have,

$$\frac{(1-\nu)}{2}\frac{\partial^2 f_n}{\partial\theta^2}+\left\{\frac{n(1+\nu)}{4}-\frac{(3-\nu)}{2}\right\}\frac{\partial g_n}{\partial\theta}+\left(\frac{n^2}{4}-1\right)f_n = \frac{5(1-\nu)}{h^2}\left[\left(\frac{n}{2}-1\right)h_{n-2}+f_{n-4}\right], \tag{21}$$

$$\frac{\partial^2 g_n}{\partial\theta^2}+\left[\frac{(3-\nu)}{2}+\frac{n(1+\nu)}{4}\right]\frac{\partial f_n}{\partial\theta}+\frac{(1-\nu)}{2}\left(\frac{n^2}{4}-1\right)g_n = \frac{5(1-\nu)}{h^2}\left(\frac{\partial h_{n-2}}{\partial\theta}+g_{n-4}\right), \tag{22}$$

$$\frac{\partial^2 h_n}{\partial\theta^2}+\frac{n^2 h_n}{4}=-\frac{n}{2}f_{n-2}-\frac{\partial g_{n-2}}{\partial\theta}, \tag{23}$$

and

$$M_{rr}=\frac{1}{1-\nu}\sum_{n=0}^{\infty}r^{n/2-1}\left[\left(\frac{n}{2}+\nu\right)f_n(\theta)+\nu\frac{\partial g_n(\theta)}{\partial\theta}\right], \tag{24}$$

$$M_{\theta\theta}=\frac{1}{1-\nu}\sum_{n=0}^{\infty}r^{n/2-1}\left[\left(1+\frac{n\nu}{2}\right)f_n(\theta)+\frac{\partial g_n(\theta)}{\partial\theta}\right], \tag{25}$$

$$M_{r\theta}=\frac{1}{2}\sum_{n=0}^{\infty}r^{n/2-1}\left[\left(\frac{n}{2}-1\right)g_n(\theta)+\frac{\partial f_n(\theta)}{\partial\theta}\right], \tag{26}$$

$$Q_r=\frac{5}{h^2}\sum_{n=0}^{\infty}r^{n/2-1}\left(\frac{n}{2}h_n(\theta)+f_{n-2}(\theta)\right), \tag{27}$$

$$Q_\theta=\frac{5}{h^2}\sum_{n=0}^{\infty}r^{n/2-1}\left(\frac{\partial h_n(\theta)}{\partial\theta}+g_{n-2}(\theta)\right). \tag{28}$$

To obtain the solution of the set of ordinary differential equations (21-23), one can observe that the third equation (23) can be solved separately from the first two equations (21-22). Furthermore the eigenvectors can be determined by combining the complementary functions and the particular integrals.

Considering the homogenous part of equations (21-23), the complementary functions for f_n and g_n can be shown to be

$$f_n^c = c_1\cos(1-n/2)\theta + c_2\sin(1-n/2)\theta + c_3\cos(1+n/2)\theta + c_4\sin(1+n/2)\theta \tag{29}$$

$$g_n^c = d_1\cos(1-n/2)\theta + d_2\sin(1-n/2)\theta + d_3\cos(1+n/2)\theta + d_4\sin(1+n/2)\theta \tag{30}$$

where c_i and d_i $(i = 1,2,3,4)$ are arbitrary constants. The relations between the constants are found by substituting equations (29-30) into (13) which yields (except for n=2),

$$d_1 = \frac{-6-n+(2-n)\nu}{-6+n+(2+n)\nu}c_2, \quad d_2 = \frac{-6-n+(2-n)\nu}{-6+n+(2+n)\nu}c_1,$$

$$d_3 = c_4 \quad \text{and} \quad d_4 = -c_3. \tag{31}$$

Letting

$$c_1 = [-6+n+(2+n)\nu]b_n^{(1)}, \quad c_2 = [-6+n+(2+n)\nu]b_n^{(2)},$$

$$c_3 = a_n^{(1)} \quad \text{and} \quad c_4 = a_n^{(2)} \tag{32}$$

and by substituting equation (29 and 30) into the boundary conditions at the crack faces, we have additional relations for $a_n^{(i)}$ and $b_n^{(i)}$. Finally the general complementary functions are given as,

$$f_n^c = a_n^{(1)}[\cos(1+n/2)\theta + \frac{(6-n-2\nu-n\nu)}{(2(-1)^n+n)(1+\nu)}\cos(1-n/2)\theta] + a_n^{(2)}[\sin(1+n/2)\theta + \frac{(-6+n+2\nu+n\nu)}{(-2(-1)^n+n)(1+\nu)}\sin(1-n/2)\theta] \tag{33}$$

$$g_n^c = -a_n^{(1)}[\sin(1+n/2)\theta + \frac{(6+n-2\nu+n\nu)}{(2(-1)^n+n)(1+\nu)}\sin(1-n/2)\theta] + a_n^{(2)}[\cos(1+n/2)\theta + \frac{(6+n-2\nu+n\nu)}{(2(-1)^n-n)(1+\nu)}\cos(1-n/2)\theta]. \tag{34}$$

By solving (23), the complementary function of h_n^c is given as

$$h_n^c = a_n^{(3)}\left[\frac{(1+(-1)^n)}{2}\cos(n/2)\theta + \frac{(1-(-1)^n)}{2}\sin(n/2)\theta\right]. \qquad (35)$$

The complementary functions just derived would be used as the global displacement interpolation function. It is found that the numerical results become highly accurate when the complementary functions alone are chosen.

In addition, when the particular integrals of equations are determined, the truncated complete infinite series of up to the eighth term are obtained and are expressed in the Appendix. It is important to realize that in contrast to plane crack problems, the leading unknown coefficients ($a_n^{(i)}$, i=1,2,3) are coupled with the higher order coefficients through the equilibrium equations. Therefore the determination of the coefficients is in fact solving a non-linear problem that requires an iterative solution procedure. However, it can be observed from equations (A.1) that the non-linear effects become insignificant when the region shrinks toward the crack tip or the thickness of plate increases to infinity. To avoid the troublesome iterative solution, only the complementary functions and a sufficiently small singular zone will be considered in the subsequent fractal transformation. Finally, by substituting the displacement equations (18-20) into (24-28), the plate forces can be derived. In particular, when n=1, the singular force components are given by,

$$M_{r1} = \frac{1}{2\sqrt{r}}\left[a_1^{(1)}\left(\cos\frac{3\theta}{2} - 5\cos\frac{\theta}{2}\right) + a_1^{(2)}\left(\sin\frac{3\theta}{2} - \frac{5}{3}\sin\frac{\theta}{2}\right)\right]$$

$$M_{\theta 1} = \frac{1}{2\sqrt{r}}\left[-a_1^{(1)}\left(\cos\frac{3\theta}{2} + 3\cos\frac{\theta}{2}\right) - a_1^{(2)}\left(\sin\frac{3\theta}{2} + \sin\frac{\theta}{2}\right)\right]$$

$$M_{r\theta 1} = \frac{1}{2\sqrt{r}}\left[-a_1^{(1)}\left(\sin\frac{3\theta}{2} + \sin\frac{\theta}{2}\right) + a_1^{(2)}\left(\cos\frac{3\theta}{2} + \frac{1}{2}\cos\frac{\theta}{2}\right)\right]$$

$$Q_{r1} = \frac{5}{2h^2\sqrt{r}}a_1^{(3)}\sin\frac{\theta}{2}$$

$$Q_{\theta 1} = \frac{5}{2h^2\sqrt{r}} a_1^{(3)} \cos\frac{\theta}{2}. \tag{36}$$

The distributions of shear forces and moments for Reissner plate are found to be similar to the counter-parts of the stress components of the three-dimensional straight crack as derived by Hartranft and Sih [29]. The displacement and rotation fields could be determined by substituting the eigenfunctions as shown in the Appendix into the equations (18) to (20).

2.2. Fracture parameters

Following the definitions of the fracture parameters by Irwin [30], moment intensity factors K_1 and K_2, and shear force intensity factor K_3 are given as follows:

$$\begin{aligned} K_1 &= \lim_{r\to 0} \sqrt{2r}\, M_{22}(r,0), \\ K_2 &= \lim_{r\to 0} \sqrt{2r}\, M_{12}(r,0), \\ K_3 &= \lim_{r\to 0} \sqrt{2r} Q_2(r,0). \end{aligned} \tag{37}$$

Explicit dependence of the stress intensity factors $K_i(x_3), (i = I, II, III)$ on the transverse coordinate x_3 is obtained by means of the relations

$$K_I(x_3) = \frac{12x_3}{h^3} K_1 ,$$

$$K_{II}(x_3) = \frac{12x_3}{h^3} K_2 ,$$

and $$K_{III}(x_3) = \frac{3}{2h}\left[1 - \left(\frac{2x_3}{h}\right)^2\right] K_3. \tag{38}$$

Considering the singular forces (36) and the definitions of (37), the moment intensity factors and shear intensity factor can further be related to the unknown coefficients as,

$$K_1 = -2\sqrt{2} a_1^{(1)}, \quad K_2 = -\frac{2\sqrt{2}}{3} a_1^{(2)} \quad \text{and} \quad K_3 = \frac{5\sqrt{2}}{2h^2} a_1^{(3)}. \tag{39}$$

Thus, the whole problem is reduced to the determination of coefficients $a_1^{(i)}$.

3. Decomposition of Stiffness Matrix for Reissner Plate Elements

Consider an *m*-node Reissner plate isoparametric element, the coordinates and the displacements of which may be expressed by

$$x_1 = \sum_{i=1}^{m} N_i(\xi,\eta) X_{1i} \quad \text{and} \quad x_2 = \sum_{i=1}^{m} N_i(\xi,\eta) X_{2i} \tag{40}$$

and

$$\psi_1 = \sum_{i=1}^{m} N_i(\xi,\eta)\psi_{1i} \ , \ \psi_2 = \sum_{i=1}^{m} N_i(\xi,\eta)\psi_{2i}$$

and $$w = \sum_{i=1}^{m} N_i(\xi,\eta) w_i \tag{41}$$

where (X_{1i}, X_{2i}) and (ψ_{1i},ψ_{2i},w_i) are the nodal coordinates and nodal displacements of an element respectively and $N_i(\xi,\eta)$ are the shape functions. The resulting element stiffness equation is

$$\mathbf{Kd} = \mathbf{Q}. \tag{42}$$

The stiffness matrix **K** may be calculated by

$$\mathbf{K} = \int_{-1}^{1}\int_{-1}^{1} \mathbf{B}^T \mathbf{D}\mathbf{B} \det[\mathbf{J}] d\xi d\eta \,. \tag{43}$$

In particular, the load vector **Q** for uniformly distributed load with intensity *p* may be expressed as

$$\mathbf{Q} = \int_{-1}^{1} \mathbf{N}^T p \mathbf{det}[\mathbf{J}] d\xi d\eta \tag{44}$$

where

$$\mathbf{B}=\begin{bmatrix} -\dfrac{\partial \mathbf{N}}{\partial x_1} & \mathbf{0} & \mathbf{0} \\ \mathbf{0} & -\dfrac{\partial \mathbf{N}}{\partial x_2} & \mathbf{0} \\ -\dfrac{\partial \mathbf{N}}{\partial x_2} & -\dfrac{\partial \mathbf{N}}{\partial x_1} & \mathbf{0} \\ -\mathbf{N} & \mathbf{0} & \dfrac{\partial \mathbf{N}}{\partial x_1} \\ \mathbf{0} & -\mathbf{N} & \dfrac{\partial \mathbf{N}}{\partial x_2} \end{bmatrix} \tag{45}$$

$$\mathbf{J}=\begin{bmatrix} \dfrac{\partial x_1}{\partial \xi} & \dfrac{\partial x_2}{\partial \xi} \\ \dfrac{\partial x_1}{\partial \eta} & \dfrac{\partial x_2}{\partial \eta} \end{bmatrix} \tag{46}$$

$$\mathbf{D}=\begin{bmatrix} D & \nu D & & & \\ \nu D & D & & \mathbf{0} & \\ & & \dfrac{1-\nu}{2}D & & \\ & \mathbf{0} & & \dfrac{h}{1.2}\mu & \\ & & & & \dfrac{h}{1.2}\mu \end{bmatrix} \tag{47}$$

where μ is the shear modulus.

Considering two elements denoted by *1* and *2*, which are similar in x_1 and x_2 directions such that $X_{1i}^2 = \bar{\xi} X_{1i}^1$ and $X_{2i}^2 = \bar{\xi} X_{2i}^1$ in which $\bar{\xi}$ is the proportionality constant. By equation (46), one can have

$$\mathbf{det}[\mathbf{J}^2] = \bar{\xi}^2 \mathbf{det}[\mathbf{J}^1]. \tag{48}$$

The stiffness matrix **K** in (43) for element *2* can be decomposed according to the power of $\bar{\xi}$ to three sub-matrices $\mathbf{S}_0$, $\mathbf{S}_1$ and $\mathbf{S}_2$, such that

$$\mathbf{K}^2 = \int_{-1}^{1}\int_{-1}^{1} \mathbf{B}^{2T}\mathbf{D}\mathbf{B}^2 \mathbf{det}[\mathbf{J}^2] d\xi d\eta = \mathbf{S}_0 + \bar{\xi}\mathbf{S}_1 + \bar{\xi}^2\mathbf{S}_2 \tag{49}$$

where

$$\mathbf{S}_0 = \int_{-1}^{1}\int_{-1}^{1} \begin{bmatrix} D\dfrac{\partial \mathbf{N}^T}{\partial x_1^1}\dfrac{\partial \mathbf{N}}{\partial x_1^1} + \dfrac{1-\nu}{2}D\dfrac{\partial \mathbf{N}^T}{\partial x_2^1}\dfrac{\partial \mathbf{N}}{\partial x_2^1} & \nu D\dfrac{\partial \mathbf{N}^T}{\partial x_1^1}\dfrac{\partial \mathbf{N}}{\partial x_2^1} + \dfrac{1-\nu}{2}D\dfrac{\partial \mathbf{N}^T}{\partial x_2^1}\dfrac{\partial \mathbf{N}}{\partial x_1^1} & \mathbf{0} \\ \nu D\dfrac{\partial \mathbf{N}^T}{\partial x_2^1}\dfrac{\partial \mathbf{N}}{\partial x_1^1} + \dfrac{1-\nu}{2}D\dfrac{\partial \mathbf{N}^T}{\partial x_1^1}\dfrac{\partial \mathbf{N}}{\partial x_2^1} & D\dfrac{\partial \mathbf{N}^T}{\partial x_2^1}\dfrac{\partial \mathbf{N}}{\partial x_2^1} + \dfrac{1-\nu}{2}D\dfrac{\partial \mathbf{N}^T}{\partial x_1^1}\dfrac{\partial \mathbf{N}}{\partial x_1^1} & \mathbf{0} \\ \mathbf{0} & \mathbf{0} & \dfrac{h\mu}{1.2}\dfrac{\partial \mathbf{N}^T}{\partial x_1^1}\dfrac{\partial \mathbf{N}}{\partial x_1^1} + \dfrac{h\mu}{1.2}\dfrac{\partial \mathbf{N}^T}{\partial x_2^1}\dfrac{\partial \mathbf{N}}{\partial x_2^1} \end{bmatrix} \mathbf{det}[\mathbf{J}^1]d\xi d\eta \tag{50}$$

$$\mathbf{S}_1 = \int_{-1}^{1}\int_{-1}^{1} \begin{bmatrix} \mathbf{0} & \mathbf{0} & -\dfrac{h\mu}{1.2}\mathbf{N}^T\dfrac{\partial \mathbf{N}}{\partial x_1^1} \\ \mathbf{0} & \mathbf{0} & -\dfrac{h\mu}{1.2}\mathbf{N}^T\dfrac{\partial \mathbf{N}}{\partial x_2^1} \\ -\dfrac{h\mu}{1.2}\dfrac{\partial \mathbf{N}^T}{\partial x_1^1}\mathbf{N} & -\dfrac{h\mu}{1.2}\dfrac{\partial \mathbf{N}^T}{\partial x_2^1}\mathbf{N} & \mathbf{0} \end{bmatrix} \mathbf{det}[\mathbf{J}^1]d\xi d\eta \tag{51}$$

and

$$\mathbf{S}_2 = \int_{-1}^{1}\int_{-1}^{1} \begin{bmatrix} \dfrac{h\mu}{1.2}\mathbf{N}^T\mathbf{N} & \mathbf{0} & \mathbf{0} \\ \mathbf{0} & \dfrac{h\mu}{1.2}\mathbf{N}^T\mathbf{N} & \mathbf{0} \\ \mathbf{0} & \mathbf{0} & \mathbf{0} \end{bmatrix} \mathbf{det}[\mathbf{J}^1]d\xi d\eta . \tag{52}$$

Similarly, the associate load vector can be written as

$$\mathbf{Q}^2 = \bar{\xi}^2\mathbf{Q}^1. \tag{53}$$

Equations (49) and (53) can be used to calculate any element stiffness matrix and the associate load vector with geometrical similarity.

4. Fractal Transformation for Cracked Reissner Plates

Figure 2 shows the layout of the fractal mesh. $\mathbf{\Gamma}_0$ is any convex curve that separates the singular region $\mathbf{\Psi}$ with the regular region. In the singular region, infinite many of conventional finite elements are capable of modeling the singular behavior of the crack tip. It is convenient to take the crack tip as a center of similarity as shown in Figure 2. Noting the defined range $0<\bar{\xi}<1$ of the proportionality constant, an infinite set of curves $\{\Gamma_1, \Gamma_2, \Gamma_3, ...\}$ similar to the shape of $\mathbf{\Gamma}_0$ with proportionality constants $\bar{\xi}^1, \bar{\xi}^2, \bar{\xi}^3 \ldots$ are generated inside the singular region. In between any two curves $\mathbf{\Gamma}_{n-1}$ and $\mathbf{\Gamma}_n$, the region is named the n^{th} layer. All the nodes located on the curve $\mathbf{\Gamma}_0$ are called the master nodes. A set of straight lines that emanate from the similarity center is connected to the master nodes. Therefore, each layer is divided into a mesh of element with a similar pattern. All the nodes inside the curve $\mathbf{\Gamma}_0$ are called the slave nodes. The grading of mesh inside the singular region can be controlled by the proportionality constant $\bar{\xi}<1$. Higher values of $\bar{\xi}$ will produce finer grade of mesh and vice versa. By this procedure, a fractal mesh is generated. The final stiffness matrix in the singular domain Ψ shown in Figure 2 is accomplished by transforming the stiffness matrix of the first layer of fractal mesh and modifying each entry of the stiffness matrix.

INSERT FIGURE 2 AROUND HERE

For the first layer of mesh, let the displacements on the boundary $\mathbf{\Gamma}_0$ be the masters $\mathbf{d}_m$ and the displacements within the boundary $\mathbf{\Gamma}_0$ be the slaves $\mathbf{d}_s$. To carry out the transformation, equation (42) is first partitioned with respect to *s* and *m* as,

$$\mathbf{Kd} = \begin{bmatrix} \mathbf{K}^f_{ss} & \mathbf{K}^f_{sm} \\ \mathbf{K}^f_{ms} & \mathbf{K}^f_{mm} \end{bmatrix} \begin{Bmatrix} \mathbf{d}_s \\ \mathbf{d}_m \end{Bmatrix} = \begin{Bmatrix} \mathbf{f}_s \\ \mathbf{f}_m \end{Bmatrix} \tag{54}$$

where the superscript '*f*' indicates first layer of mesh. Only the displacements at the slave nodes are transformed. The second level (global) interpolation of displacements can be written as follows,

$$\begin{Bmatrix} \mathbf{d}_s \\ \mathbf{d}_m \end{Bmatrix} = \begin{bmatrix} \mathbf{T}_s^f & \mathbf{0} \\ \mathbf{0} & \mathbf{I} \end{bmatrix} \begin{Bmatrix} \mathbf{a} \\ \mathbf{d}_m \end{Bmatrix} \tag{55}$$

where $\mathbf{I}$ is the identity matrix and $\mathbf{T}_s^f$ is the transformation matrix that can be evaluated by suitable coordinate transformation of equations (18-20). The generalized stiffness matrix and force vector for the first layer of fractal mesh can be evaluated, and the result is given by,

$$\begin{bmatrix} \mathbf{T}_s^{f\,T}\mathbf{K}_{ss}^f\mathbf{T}_s^f & \mathbf{T}_s^{f\,T}\mathbf{K}_{sm}^f \\ \mathbf{K}_{ms}^f\mathbf{T}_s^f & \mathbf{K}_{mm}^f \end{bmatrix} \begin{Bmatrix} \mathbf{a} \\ \mathbf{d}_m \end{Bmatrix} = \begin{Bmatrix} \mathbf{T}_s^{f\,T}\mathbf{f}_s \\ \mathbf{f}_m \end{Bmatrix}$$

$$\overline{\mathbf{K}}^f \overline{\mathbf{d}}^f = \overline{\mathbf{Q}}^f . \tag{56}$$

For the inner layer, each element stiffness matrix and load vector within the first layer of Ψ would be transformed and assembled. Based on the fractal concepts, an infinite number of elements and numerous degrees of freedom would virtually be generated near the crack tip. Applying the fractal transformation technique, infinitely many layers of mesh can be transformed and assembled with little effort. Inner layer of the generalized stiffness matrix and generalized load vector are given as

$$\begin{aligned} \overline{\mathbf{K}}^i &= \sum_{k=2}^{\infty} \mathbf{T}^{k\,T}\mathbf{K}^k\mathbf{T}^k \\ &= \sum_{k=2}^{\infty} \mathbf{T}^{k\,T}[\mathbf{S}_0 + \bar{\xi}^{(k-1)}\mathbf{S}_1 + \bar{\xi}^{2(k-1)}\mathbf{S}_2]\mathbf{T}^k \\ &= \sum_{l=0}^{2}\sum_{k=2}^{\infty} \bar{\xi}^{l(k-1)}\mathbf{T}^{k\,T}\mathbf{S}_l\mathbf{T}^k \quad , \end{aligned} \tag{57}$$

$$\begin{aligned} \overline{\mathbf{Q}}^i &= \sum_{k=2}^{\infty} \mathbf{T}^{k\,T}\mathbf{Q}^k \\ &= \sum_{k=2}^{\infty} \bar{\xi}^{2(k-1)}\mathbf{T}^{k\,T}\mathbf{Q}^f . \end{aligned} \tag{58}$$

Due to the fact of geometrical similarity, the transformation matrix at the k[th] layer ($\mathbf{T}^k$) can be written in term of the first layer ($\mathbf{T}^f$) i.e.,

$$\mathbf{T}^k = \mathbf{T}^f \mathbf{Diag}[\alpha_j] \tag{59}$$

where $\alpha_j = \bar{\xi}^{n_j(k-1)/2}$ and $n_j = \begin{cases} (j-1)/2 & \text{for } j = 4,7,10,\cdots \\ (j-2)/2 & \text{for } j = 5,8,11,\cdots \\ (j-3)/2 & \text{for } j = 6,9,12,\cdots \end{cases}$. (60)

Substitute equations(59) and (60) into equations (57) and (58), one can observe that the summations of infinite series in each entry of the stiffness matrix is in fact a summation of a geometric progression series. Therefore, the condensation of equation (57) can be achieved by multiplying each entry of transformed stiffness matrix at the first layer $\bar{s}_{ijl}^f$ with a factor of $\bar{\alpha}_{ijl}$, thus

$$\bar{\mathbf{K}}^i = \sum_{l=0}^{2} \begin{bmatrix} & \vdots & \\ \cdots & \bar{\alpha}_{ijl}\bar{s}_{ijl}^f & \cdots \\ & \vdots & \end{bmatrix} \tag{61}$$

where $\bar{\alpha}_{ijl} = \dfrac{1}{\bar{\xi}^{-(m_i+n_j+2l)/2} - 1}$ and $m_i = \begin{cases} (i-1)/2 & \text{for } i = 4,7,10,\cdots \\ (i-2)/2 & \text{for } i = 5,8,11,\cdots \\ (i-3)/2 & \text{for } i = 6,9,12,\cdots \end{cases}$. (62)

Similarly for the load vector

$$\bar{\mathbf{Q}}^i = \begin{Bmatrix} \vdots \\ \bar{\beta}_i \bar{q}_i^f \\ \vdots \end{Bmatrix} \tag{63}$$

in which

$$\bar{\beta}_i = \frac{1}{\bar{\xi}^{-(m_i+4)/2} - 1} \quad \text{and } m_i = \begin{cases} (i-1)/2 & \text{for } i = 1,4,7,\cdots \\ (i-2)/2 & \text{for } i = 2,5,8,\cdots \\ (i-3)/2 & \text{for } i = 3,6,9,\cdots \end{cases}. \tag{64}$$

Finally,

$$\bar{\mathbf{K}}_s = \bar{\mathbf{K}}^f + \bar{\mathbf{K}}^i, \tag{65}$$

and $\overline{\mathbf{Q}}_s = \overline{\mathbf{Q}}^f + \overline{\mathbf{Q}}^i$ (66)

The generalized stiffness matrix and the generalized load vector can be obtained easily.

5. Examples on Mode I, Mode II and Mode III Cracks

In order to verify the validity of the proposed approach, problems concerning the bending of a square plate under the effects of edge moment and twisting are studied. The results are compared with the analytical solution by Joseph[6] and Wang [4] and [5] for infinite plates. The present analyses employed 9-node Lagrange plate elements as the reliability and accuracy for this kind of elements had been ascertained by Zienkiewicz and Taylor [31].

The following data are used throughout the analyses: i) For material properties, E=20000, ν=0.3 unless otherwise specified. ii) For geometrical data, b=1 where 2b is the plate width, crack length of $2a$ is for central crack. iii) For loading condition, edge moment or edge twisting moment is of unit intensity. iv) The self-similarity ratio is assumed to be 0.5.

5.1. Infinite plate with crack subjected to out-of-plate bending

The analytical solution of infinite cracked plate subjected to out-of-plate bending had been studied by Hartranft and Sih [3], Wang [4] and recently by Joseph and Erdogan [6]. whereas the numerical solutions had been investigated by various investigators[11,12,14,16,17]. This problem is considered in this section to examine the thickness and the Poisson's ratio effects on the variations of moment intensity factors and the convergence of the F2LFEM.

Figure 3 shows the typical finite element mesh for the analysis, consisting of 152 elements and 694 nodes. Since all the applied loads are symmetric about the axis on which the crack is

lying, only one quarter of the plate requires analysis. The ratio of plate width to crack length b/a=20.0 is selected since it has been shown to be large enough for modeling the infinite plate by Barsoum [11].

INSERT FIGURE 3 AROUND HERE

In order to study the convergence of the proposed method with the size of fractal mesh r_0 (the radius of fractal mesh), five finite element meshes with size of fractal mesh r_0/a ranging from 1/16 to 1/256 are prepared. Table 1 shows the results of convergence of the dimensionless moment intensity factor $K_1 / M_0\sqrt{a}$. It is found that r_0/a<1/256 is in general, enough for achieving the convergence for the plate with thickness ratio h/b=0.01. Furthermore the convergence of number of transformation terms is also investigated. The results are tabulated in Table 2. It is found that a higher number of terms is required to achieve an accurate solution for smaller ratios of h/a. In general, 14 terms are sufficient for thin plate with h/b=1/1000 to reach a convergent solution.

	Size of fractal mesh r_0/a						
H/a	1/16	1/32	1/64	1/128	1/256	Hartanft	Haung
2.0	0.818	0.820	0.820	0.820	0.820	0.816	0.819
1.5	0.783	0.787	0.788	0.788	0.788	0.781	0.785
1.0	0.739	0.746	0.748	0.749	0.749	0.741	0.745
0.5	0.670	0.692	0.698	0.700	0.701	0.693	0.697
0.2	0.542	0.622	0.652	0.662	0.664	0.697	0.651

Table 1: Convergence of F2LFEM against size of fractal mesh.

(Number of transformation terms = 12, $\nu = 0.3$)

	Number of transformation terms							
h/a	2	4	6	8	10	12	14	16
1.0	.724	.749	.749	.749	.749	.749	.749	.749
0.1	.496	.624	.635	.637	.638	.639	.639	.639
0.02	.184	.348	.446	.466	.476	.481	.485	.485

Table 2: Convergence of F2LFEM against number of transformation terms.

(r_0/a=1/128, ν=0.3)

When compared with the F2LFEM for two-dimensional cracks, it is found that the accuracy of the solution does depend on the size of fractal mesh. Faster convergence is achieved for smaller size of fractal mesh or larger thickness of plate. It should be recalled that the global interpolating functions used here contain only the complementary functions and that all the effects of coupling coefficients in r_0 of equation (A.1) are neglected. However, the coupling effects are found to be proportional to the ratio r_0^n/h^m where n and m are some positive

integers. The coupling effects would be diminished leading to a good approximation by solely the complementary functions when the size of fractal mesh r_0 is small or the thickness of plate h is large.

Thickness effect is studied here using the size of fractal mesh of r_0/a=256 and 14 transformation terms. The dimensionless moment intensity factors are plotted in Figure 4 for comparison with those of Barsoum[11], Yagawa[12], Alwar[14], Viswanath[17] and Joseph[6]. It is found that the 3-dimensional analysis [14] generally over-estimated the moment intensity factors by around 8%. When compare with the extremely precise analytical solutions by Joseph[6], all the numerical results (Barsoum[11], Yagawa[12], Alwar[14], Viswanath[17] and the present method) under-estimate the moment intensity factors when approaching the thin plate limit. The results reported by Barsoum[11], Yagawa[12] and Viswanath[17] started to departure from the exact solution when h/a are less than 1.0, 0.5 and 0.25 respectively. The accuracy and the reliability of the present method appear to be the best among all the available numerical methods. The present numerical solutions tend to diverse from the analytical solution only when the ratio of h/a is less than 0.04 or equivalent speaking the ratio of r_0/h is greater than 1/10.

INSERT FIGURE 4 AROUND HERE

Poisson's ratio and thickness effects are studied here used the size of fractal mesh of r_0/a=256 and 14 transformation terms. The dimensionless moment intensity factors are plotted in Figure 5 for comparison with those of Wang[4]. Very good agreement with less than 1.5% difference with Wang's analytical results is obtained. A distinguishing feature of

accurate prediction of mode I moment intensity factors for a wide range of *h/a* ratios 0.04 to 5 and the full range of Poisson's ratio is observed.

INSERT FIGURE 5 AROUND HERE

5.2. Infinite plate with crack subjected to twisting bending

The solution of infinite cracked plate subjected to twist loading shown in Figure 6 had been studied analytically by Wang [5] and numerically by Huang [16]. It is a mixed mode (II and III) problem. We use the similar mesh as shown in Figure 3 with width to crack length ratio b/a=20.0 for the analyses. Since all the applied loads are skew-symmetric with respect to the axis on which the crack is lying, only one quarter of the plate is analyzed.

INSERT FIGURE 6 AROUND HERE

Poisson's ratio and the thickness effects are studied here using a fractal mesh of size r_0/a=256 and 14 transformation terms. The dimensionless moment intensity factor $K_2 / (H_0\sqrt{a})$ and shear intensity factor $K_3(1+\nu)h / (H_0\sqrt{10a})$ are compared with the results of Wang [19] and are plotted in Figure 7 and 8 for mode II and III respectively. Good agreements with deviations less than 1.0% and 5.0% for mode II and mode III respectively are observed. A distinguishing feature of accurate prediction of moment intensity factors for a wide range of *h/a* ratios (from 0.02 to 5) and full range of Poisson's ratio is also noticed.

INSERT FIGURES 7 & 8 AROUND HERE

6. Conclusion

In this paper, the F2LFEM was applied to analyze the mixed mode problems of Reissner plates with crack. The eigenfunction series of cracked Reissner plate was derived up to the eighth term. The decomposition of stiffness matrices and force vectors with similar shape was discussed. The basic formulation of the F2LFEM on the analysis of Reissner plate cracks including the fractal transformation technique was given. The convergence study of the present method showed that highly accurate results could be obtained when the fractal mesh size satisfies $r_0/h < 1/10$. Examples were given on I, II and III modes to illustrate the efficiency of the present method. In general, good accuracy of about 1.0% error for mode I and mode II, and about 5.0% error for mode III cracks were found when compared with Wang's results. A distinguishing feature of accurate prediction of moment intensity factors for a wide range of *h/a* ratios (from 0.04 to 5) and the full range of Poisson's ratio is also observed. The present approach has shown to be more reliable and accurate than the other methods such as the special crack tip element method [17] and the quarter-point element approach[11] in which errors of 10% or more were reported for decreasing plate thickness. By combining the present cracked plate formulation with the cracked membrane formulations [23] and [24], it is possible to extend the present F2LFEM to solutions of general flat shell with cracks.

Reference:

1 G.C. Sih, P.C. Paris and F. Erdogan, Crack-tip, stress intensity factors for the plane extension and plate bending problem, *Journal of Applied Mechanics*, **29** (1962), 306-312.

2 J. K. Knowles and N. M. Wang, On the bending of an elastic plate containing a crack, *Journal of Mathematics and Physics,* **39**(1960), 223-236.

3 R. J. Hartranft and G.C. Sih, Effect of plate thickness on the bending stress distribution around through cracks, *Journal of Mathematics and Physics,* **47**, (1968), 276-291.

4 N. M. Wang, Effects of plate thickness on the bending of an elastic plate containing a crack, *Journal of Mathematics and Physics*, **47** (1968), 371-390.

5 N. M. Wang, Twisting of an elastic plate containing a crack, *International Journal of Fracture Mechanics*, **6**(4)(1970), 367-378.

6 P.F. Joseph and F. Erdogan, Bending of a thin Reissner plate with a through crack, *Journal of Applied Mechanics*, 58 (1991),842-846.

7 M.J. Young and C.T. Sun, Cracked plates subjected to out-of-plane tearing loads, *International Journal of Fracture*, **60**(1993), 1-18.

8 C.Y. Hui and A.T. Zehnder, A theory for the fracture of thin plates subjected to bending and twisting moments, *International Journal of Fracture*, **61**(1993), 211-229.

9 M. V. V. Murthy, K. N. Raju and S. Viswanath, On the bending stress distribution at the tip of a stationary crack from Reissner's theory, *International Journal of Fracture*, **17**(6) (1981), 537-552.

10 H. Boduroglu and F. Erdogan, Internal and edge cracks in a plate of finite width under bending, *Journal of Applied Mechanics*, **50**(1983), 621-629.

11 R. S. Barsoum, A degenerate solid element for linear fracture analysis of plate bending and general shells, *International Journal for Numerical Methods in Engineering*, **10**(1976), 551-564.

12 G. Yagawa and T. Nishioka, Finite element analysis of stress intensity factors for plane extension and plate bending problems, *International Journal for Numerical Methods in Engineering*, **14**(1979), 727-740.

13 H. C. Rhee and S. N. Atluri, Hybrid stress finite element analysis of bending of a plate with a through flaw, *International Journal for Numerical Methods in Engineering*, **18**(1982), 259-271.

14 R. S. Alwar and K. N. Ramachandran Nambissan, Three-dimensional finite element analysis of cracked thick plates in bending, *International Journal for Numerical Methods in Engineering*, **19**(1983), 293-303.

15 N. N. Wahba, On the use of singular displacement finite elements for cracked plate in bending, *International Journal of Fracture,* **27**(1985), 3-30.

16 M. Huang and Y. Long, Calculation of stress intensity factors of cracked Reissner plates by the sub-region mixed finite element method, *Computers and Structures,* **30**(4) (1988), 837-840.

17 S. Viswanath and M. V. V. Murthy, A special crack tip element for bending of plates with through cracks from a sixth-order plate theory, *Engineering Fracture Mechanics,* **32**(1989), 91-109.

18 H. A. Sosa and J. W. Eischen, Computation of stress intensity factors for plate bending via a path-independent integral, *Engineering Fracture Mechanics,* **25**(4) (1986), 451-462.

19 S. Viswanath, H. V. Lakshminarayana and D. D. Ravindranath, A modified crack closure integral method for calculating stress intensity factors for cracked plates subject to bending loads, *International Journal of Fracture,* **41**(1989), R45-50.

20 A. Y. T. Leung and R. K. L. Su, Fractal two-level finite element analysis of cracked Reissner's plate, *Thin Walled Structures*, 24(1996), 315-334

21 A. Y. T. Leung and R. K. L. Su, Fractal two-level finite element method for cracked classical plates using DKT elements, *Engineering Fracture Mechanics,* **54**(5) (1996), 703-711.

22 A. Y. T. Leung and R. K. L. Su, Mode I crack problems by fractal two-level finite element methods, *Engineering Fracture Mechanics,* **48**(6) (1994**),** 847-856.

23 A. Y. T. Leung and R. K. L. Su, Mixed mode two-dimensional crack problems by fractal two-level finite element method, *Engineering Fracture Mechanics*, **51**(6) (1995), 889-895.

24 A. Y. T. Leung and R. K. L. Su, Body-force linear elastic stress intensity factor calculation using fractal two-level finite element method, *Engineering Fracture Mechanics*, **51**(6) (1995), 879-888.

25 M. V. V. Murthy, S. Viswanath, A. V. Krishna Murty and K. P. Rao, A two-dimensional model for crack closure effect in plates under bending, *Engineering Fracture Mechanics,* **29**(4) (1988), 435-452.

26 P.F. Joseph and F. Erdogan, Surface crack problems in plates, *International Journal of Fracture,* **41**(1989), 105-131.

27 M.J. Young and C.T. Sun, On the strain energy release rate for a cracked plate subjected to out-of-plane bending moment, *International Journal of Fracture*, **60**(1993), 227-247.

28 H.A. Sosa, *On The Analysis of Bars, Beams and Plates with Defects, Ph.D. Thesis*, Stanford University (1986).

29 R.J. Hartranft and G.C. Sih, The use of eigenfunction expansions in general solution of three-dimensional crack problem, *Journal of Mathematics and Mechanics,* **19**(2) (1969) 123-138.

30 G.R. Irwin, Analysis of stresses and strains near the end of a crack transversing a plate, *Journal of Applied Mechanics*, **24** (1957) 361-364.

31 O. C. Zienkiewicz and R. L. Taylor, *The Finite Element Method,* Fourth edition, 2, McGraw

Appendix

For n=0

$$f_0 = a_0^{(1)} \cos\theta + a_0^{(2)} \sin\theta$$

$$g_0 = -a_0^{(1)} \sin\theta + a_0^{(2)} \cos\theta$$

$$h_0 = a_0^{(3)}$$

For n=1

$$f_1 = a_1^{(1)}\left[\cos\frac{3\theta}{2} - \frac{(5-3\nu)}{(1+\nu)}\cos\frac{\theta}{2}\right] + a_1^{(2)}\left[\sin\frac{3\theta}{2} - \frac{(5-3\nu)}{3(1+\nu)}\sin\frac{\theta}{2}\right]$$

$$g_1 = -a_1^{(1)}\left[\sin\frac{3\theta}{2} - \frac{(7-\nu)}{(1+\nu)}\sin\frac{\theta}{2}\right] + a_1^{(2)}\left[\cos\frac{3\theta}{2} - \frac{(7-\nu)}{3(1+\nu)}\cos\frac{\theta}{2}\right]$$

$$h_1 = a_1^{(3)} \sin\frac{\theta}{2}$$

For n=2

$$f_2 = a_2^{(1)}\left[\cos 2\theta + \frac{(1-\nu)}{(1+\nu)}\right]$$

$$g_2 = -a_2^{(1)} \sin 2\theta + a_2^{(2)}$$

$$h_2 = a_2^{(3)} \cos\theta - a_0^{(2)} \sin\theta$$

For n=3

$$f_3 = a_3^{(1)}\left[\cos\frac{5\theta}{2} + \frac{(3-5\nu)}{(1+\nu)}\cos\frac{\theta}{2}\right] + a_3^{(2)}\left[\sin\frac{5\theta}{2} + \frac{(3-5\nu)}{5(1+\nu)}\sin\frac{\theta}{2}\right] + a_1^{(3)}\frac{4}{3(1+\nu)h^2}\sin\frac{\theta}{2}$$

$$g_3 = -a_3^{(1)}\left[\sin\frac{5\theta}{2} - \frac{(9+\nu)}{(1+\nu)}\sin\frac{\theta}{2}\right] + a_3^{(2)}\left[\cos\frac{5\theta}{2} - \frac{(9+\nu)}{5(1+\nu)}\cos\frac{\theta}{2}\right] + a_1^{(3)}\frac{4(2+3\nu)}{3(1+\nu)h^2}\cos\frac{\theta}{2}$$

$$h_3 = a_3^{(3)} \sin\frac{3\theta}{2} + a_1^{(1)}\left[\frac{-2(7+\nu)}{3(1+\nu)}\cos\frac{3\theta}{2} + \frac{2(1-\nu)}{(1+\nu)}\cos\frac{\theta}{2}\right] + a_1^{(2)}\frac{2(1-\nu)}{3(1+\nu)}\sin\frac{\theta}{2}$$

For n=4

$$f_4 = a_4^{(1)}\left[\cos 3\theta + \frac{(1-3\nu)}{3(1+\nu)}\cos\theta\right] + a_4^{(2)}\left[\sin 3\theta + \frac{(1-3\nu)}{(1+\nu)}\sin\theta\right]$$

$$g_4 = -a_4^{(1)}\left[\sin 3\theta - \frac{(5+\nu)}{3(1+\nu)}\sin\theta\right] + a_4^{(2)}\left[\cos 3\theta - \frac{(5+\nu)}{(1+\nu)}\cos\theta\right]$$

$$h_4 = a_4^{(3)}\cos 2\theta - a_2^{(1)}\frac{(1-\nu)}{2(1+\nu)} - a_2^{(2)}\frac{1}{2}\sin 2\theta$$

For n=5

$$f_5 = a_5^{(1)}\left[\cos\frac{7\theta}{2} + \frac{(1-7\nu)}{3(1+\nu)}\cos\frac{3\theta}{2}\right] + a_5^{(2)}\left[\sin\frac{7\theta}{2} + \frac{(1-7\nu)}{7(1+\nu)}\sin\frac{3\theta}{2}\right] + a_3^{(3)}\frac{12}{7(1+\nu)h^2}\sin\frac{3\theta}{2} - a_1^{(1)}\frac{1}{3(1+\nu)h^2}\left[5\cos\frac{\theta}{2} + \frac{(61+5\nu)}{3(1+\nu)}\cos\frac{3\theta}{2}\right] - a_1^{(2)}\frac{1}{9(1+\nu)h^2}\left[5\sin\frac{\theta}{2} - \frac{(77+37\nu)}{7(1+\nu)}\sin\frac{3\theta}{2}\right]$$

$$g_5 = -a_5^{(1)}\left[\sin\frac{7\theta}{2} - \frac{(11+3\nu)}{3(1+\nu)}\sin\frac{3\theta}{2}\right] + a_5^{(2)}\left[\cos\frac{7\theta}{2} - \frac{(11+3\nu)}{7(1+\nu)}\cos\frac{3\theta}{2}\right] + a_3^{(3)}\frac{4(2+5\nu)}{7(1+\nu)h^2}\cos\frac{3\theta}{2} + a_1^{(1)}\frac{1}{3(1+\nu)h^2}\left[35\sin\frac{\theta}{2} + \frac{7(7+15\nu)}{3(1+\nu)}\sin\frac{3\theta}{2}\right] - a_1^{(2)}\frac{1}{9(1+\nu)h^2}\left[35\cos\frac{\theta}{2} - \frac{(-7+153\nu+120\nu^2)}{7(1+\nu)}\cos\frac{3\theta}{2}\right]$$

$$h_5 = a_5^{(3)}\sin\frac{5\theta}{2} + a_3^{(1)}\left[\frac{-2(1-\nu)}{(1+\nu)}\cos\frac{\theta}{2} + \frac{2(9-\nu)}{5(1+\nu)}\cos\frac{5\theta}{2}\right] - a_3^{(2)}\frac{2(1-\nu)}{5(1+\nu)}\sin\frac{\theta}{2} - a_1^{(3)}\frac{(1-\nu)}{3(1+\nu)h^2}\sin\frac{\theta}{2}$$

For n=6

$$f_6 = a_6^{(1)}\left[\cos 4\theta - \frac{\nu}{(1+\nu)}\cos 2\theta\right] + a_6^{(2)}\left[\sin 4\theta - \frac{2\nu}{(1+\nu)}\sin 2\theta\right]$$
$$+ a_4^{(3)}\frac{5}{3(1+\nu)h^2}\cos 2\theta + a_2^{(1)}\frac{5}{6(1+\nu)h^2}\cos 2\theta$$
$$- a_2^{(2)}\frac{5}{6(1+\nu)h^2}\sin 2\theta$$

$$g_6 = -a_6^{(1)}\left[\sin 4\theta - \frac{(3+\nu)}{2(1+\nu)}\sin 2\theta\right] + a_6^{(2)}\left[\cos 4\theta - \frac{(3+\nu)}{(1+\nu)}\cos 2\theta\right]$$
$$- a_4^{(3)}\frac{5(1+3\nu)}{6(1+\nu)h^2}\sin 2\theta - a_2^{(1)}\frac{5(1+3\nu)}{12(1+\nu)h^2}\sin 2\theta$$
$$+ a_2^{(2)}\frac{5}{4h^2}\left[1 - \frac{(1+3\nu)}{3(1+\nu)}\cos 2\theta\right]$$

$$h_6 = a_6^{(3)}\cos 3\theta - a_4^{(1)}\frac{(1-\nu)}{3(1+\nu)}\cos\theta - a_4^{(2)}\left[\frac{(1-\nu)}{(1+\nu)}\sin\theta - \frac{(5-\nu)}{3(1+\nu)}\sin 3\theta\right]$$

For n=7

$$f_7 = a_7^{(1)}\left[\cos\frac{9\theta}{2} - \frac{(1+9\nu)}{5(1+\nu)}\cos\frac{5\theta}{2}\right] + a_7^{(2)}\left[\sin\frac{9\theta}{2} - \frac{(1+9\nu)}{9(1+\nu)}\sin\frac{5\theta}{2}\right]$$
$$+ a_5^{(3)}\frac{100}{63(1+\nu)h^2}\sin\frac{5\theta}{2} - a_3^{(1)}\frac{1}{(1+\nu)h^2}\left[\cos\frac{\theta}{2} - \frac{(233+7\nu)}{35(1+\nu)}\cos\frac{5\theta}{2}\right]$$
$$- a_3^{(2)}\frac{1}{5(1+\nu)h^2}\left[\sin\frac{\theta}{2} - \frac{(207+263\nu)}{63(1+\nu)}\sin\frac{5\theta}{2}\right]$$
$$+ a_1^{(3)}\frac{(3+5\nu)}{12(1+\nu)h^4}\left[\sin\frac{\theta}{2} - \frac{(1+9\nu)}{9(1+\nu)}\sin\frac{5\theta}{2}\right]$$

$$g_7 = -a_7^{(1)}\left[\sin\frac{9\theta}{2} - \frac{(13+5\nu)}{5(1+\nu)}\sin\frac{5\theta}{2}\right] + a_7^{(2)}\left[\cos\frac{9\theta}{2} - \frac{(13+5\nu)}{9(1+\nu)}\cos\frac{5\theta}{2}\right]$$
$$+ a_5^{(3)}\frac{20(2+7\nu)}{63(1+\nu)h^2}\cos\frac{5\theta}{2} + a_3^{(1)}\frac{9}{(1+\nu)h^2}\left[\sin\frac{\theta}{2} - \frac{(11+35\nu)}{35(1+\nu)}\sin\frac{5\theta}{2}\right]$$
$$- a_3^{(2)}\frac{1}{5(1+\nu)h^2}\left[9\cos\frac{\theta}{2} - \frac{(171+395\nu+280\nu^2)}{63(1+\nu)}\cos\frac{5\theta}{2}\right]$$
$$+ a_1^{(3)}\frac{(3+5\nu)}{4(1+\nu)h^4}\left[3\cos\frac{\theta}{2} - \frac{(13+5\nu)}{27(1+\nu)}\cos\frac{5\theta}{2}\right]$$

$$h_7 = a_7^{(3)} \sin\frac{7\theta}{2} + a_5^{(1)}\left[\frac{-2(1-\nu)}{3(1+\nu)}\cos\frac{3\theta}{2} + \frac{2(11-3\nu)}{21(1+\nu)}\cos\frac{7\theta}{2}\right]$$
$$- a_5^{(2)}\frac{2(1-\nu)}{7(1+\nu)}\sin\frac{3\theta}{2} - a_3^{(3)}\frac{3(1-\nu)}{7(1+\nu)h^2}\sin\frac{3\theta}{2}$$
$$+ a_1^{(1)}\frac{2}{9(1+\nu)^2h^2}\left[7(1-\nu)\cos\frac{3\theta}{2} - (11-3\nu)\cos\frac{7\theta}{2}\right]$$
$$- a_1^{(2)}\frac{2(1-\nu)(14+9\nu)}{63(1+\nu)^2h^2}\sin\frac{3\theta}{2}$$

For n=8

$$f_8 = a_8^{(1)}\left[\cos 5\theta - \frac{(1+5\nu)}{5(1+\nu)}\cos 3\theta\right] + a_8^{(2)}\left[\sin 5\theta - \frac{(1+5\nu)}{3(1+\nu)}\sin 3\theta\right]$$
$$+ a_6^{(3)}\frac{3}{2(1+\nu)h^2}\cos 3\theta - a_4^{(1)}\frac{1}{9(1+\nu)h^2}\left[\frac{5}{2}\cos\theta - \frac{(5+7\nu)}{(1+\nu)}\cos 3\theta\right]$$
$$- a_4^{(2)}\frac{5}{6(1+\nu)h^2}\left[\sin\theta - \frac{(11+\nu)}{3(1+\nu)}\sin 3\theta\right]$$

$$g_8 = -a_8^{(1)}\left[\sin 5\theta - \frac{(7+3\nu)}{5(1+\nu)}\sin 3\theta\right] + a_8^{(2)}\left[\cos 5\theta - \frac{(7+3\nu)}{3(1+\nu)}\cos 3\theta\right] -$$
$$a_6^{(3)}\frac{(1+4\nu)}{2(1+\nu)h^2}\sin 3\theta + a_4^{(1)}\frac{1}{9(1+\nu)h^2}\left[\frac{25}{2}\sin\theta - \frac{(5+9\nu+6\nu^2)}{(1+\nu)}\sin 3\theta\right]$$
$$- a_4^{(2)}\frac{25}{6(1+\nu)h^2}\left[\cos\theta - \frac{(1+3\nu)}{3(1+\nu)}\cos 3\theta\right]$$

$$h_8 = a_8^{(3)}\cos 4\theta - a_6^{(1)}\frac{(1-\nu)}{4(1+\nu)}\cos 2\theta$$
$$- a_6^{(2)}\frac{1}{4(1+\nu)}\left[2(1-\nu)\sin 2\theta - (3-\nu)\sin 4\theta\right]$$
$$- a_4^{(3)}\frac{5(1-\nu)}{12(1+\nu)h^2}\cos 2\theta - a_2^{(1)}\frac{5(1-\nu)}{24(1+\nu)h^2}\cos 2\theta$$
$$+ a_2^{(2)}\frac{5}{48(1+\nu)h^2}\left[2(1-\nu)\sin 2\theta - (3-\nu)\sin 4\theta\right]$$

(A.1)

List of Captions

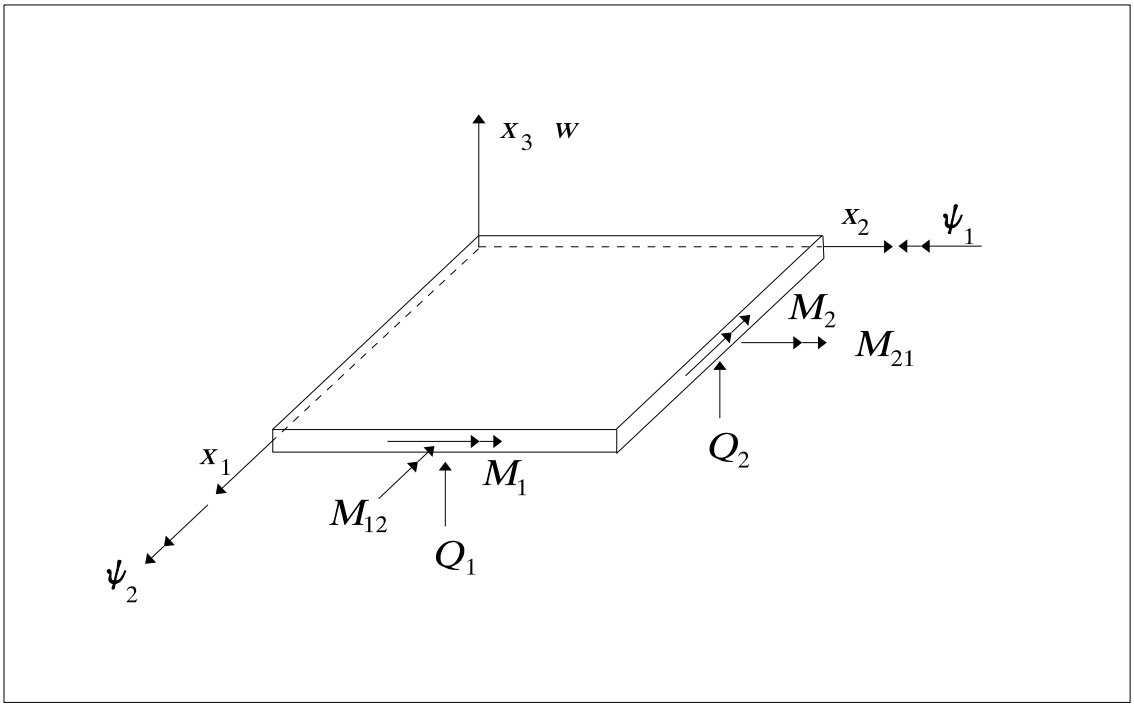

Figure 1. Notations for Reissner's plate.

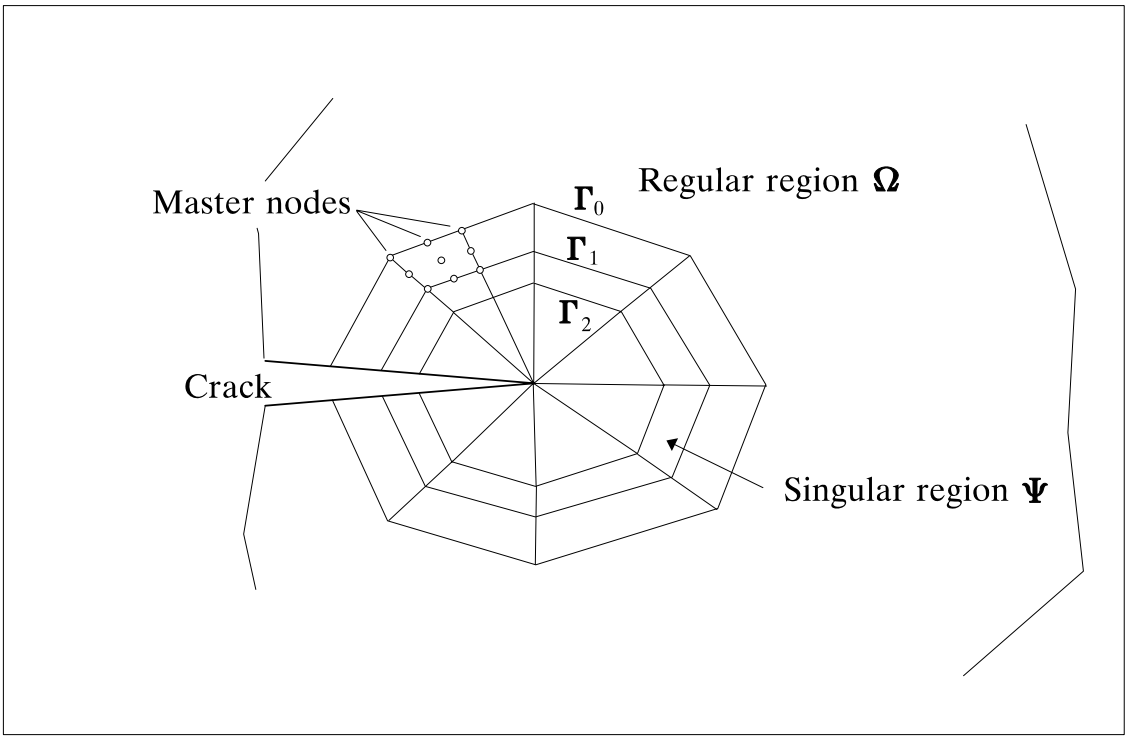

Figure 2. Fractal mesh configuration.

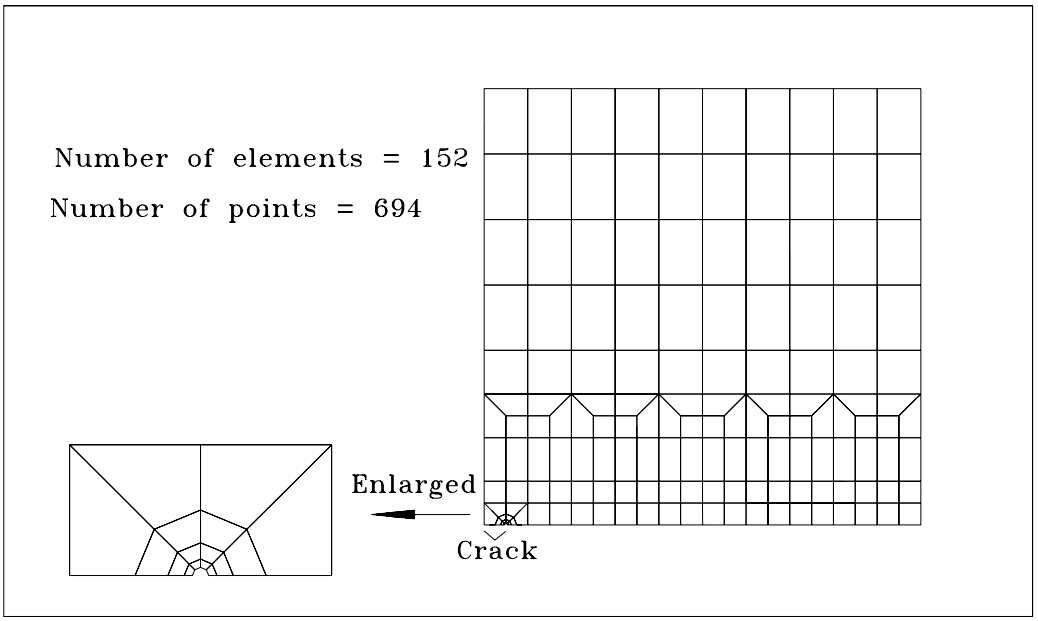

Figure 3. Mesh configuration for modeling the infinite plate.

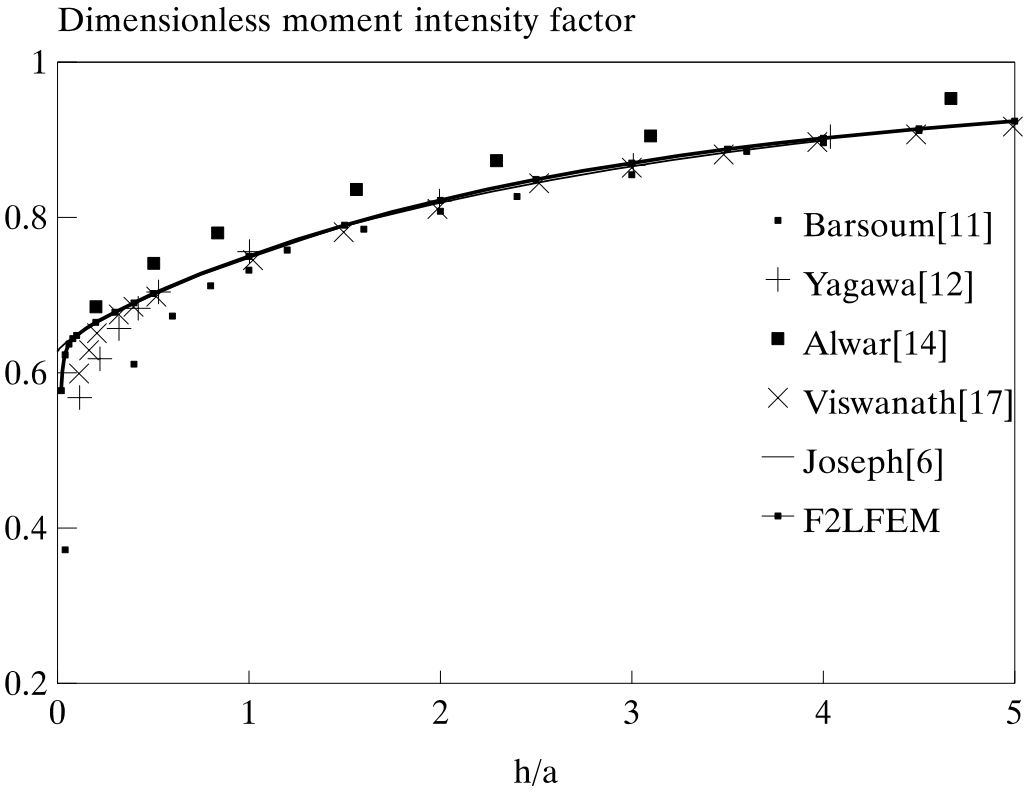

Figure 4. Comparison of moment intensity factors.

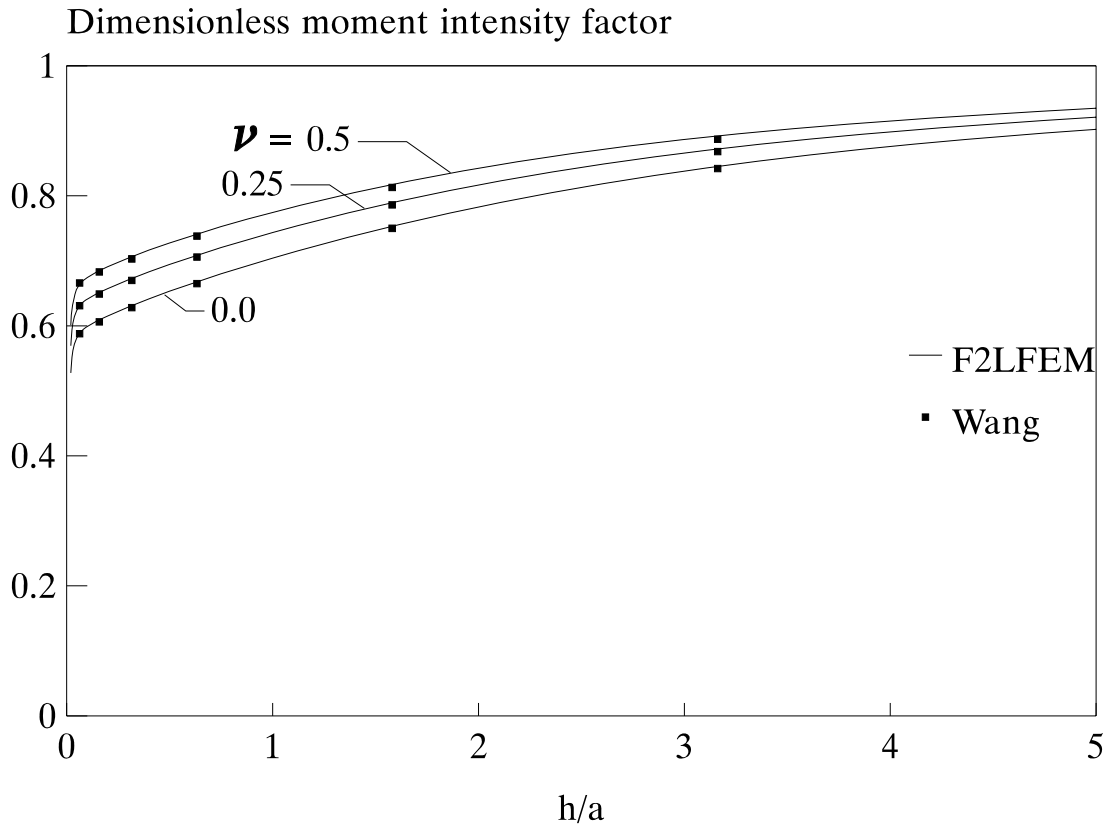

Figure 5. Variation of K1 versus ratio of plate thickness to crack length.

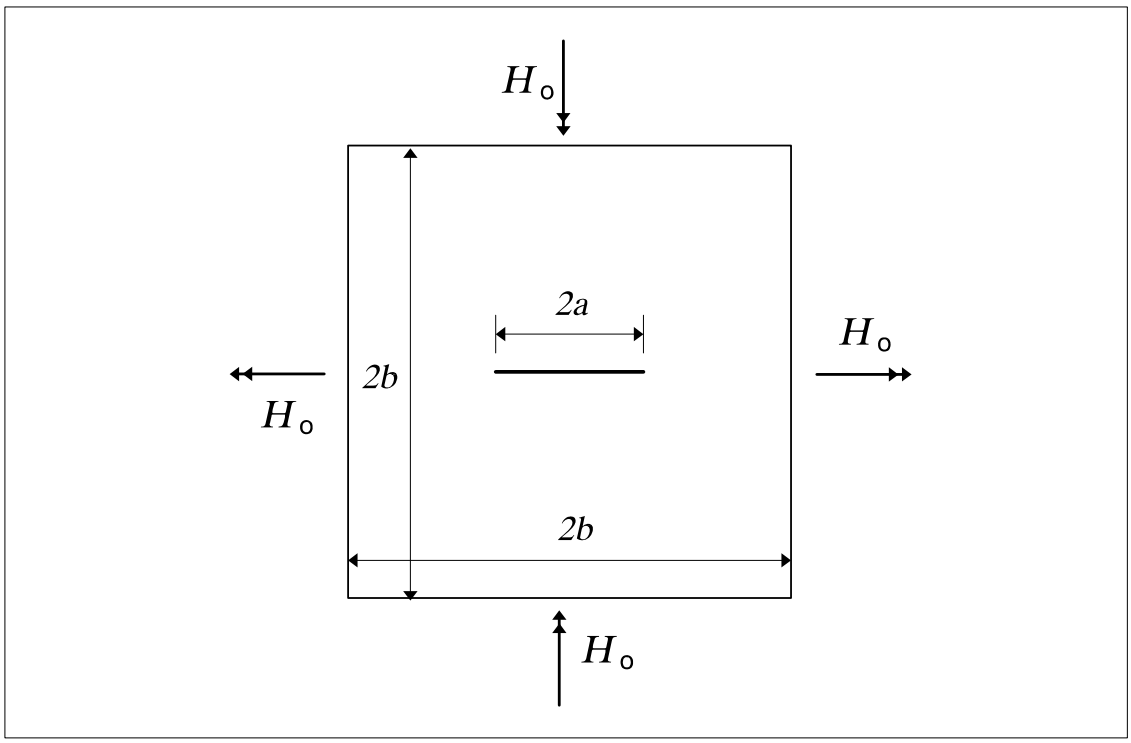

Figure 6. Centre cracked plate subjected to twisting moment.

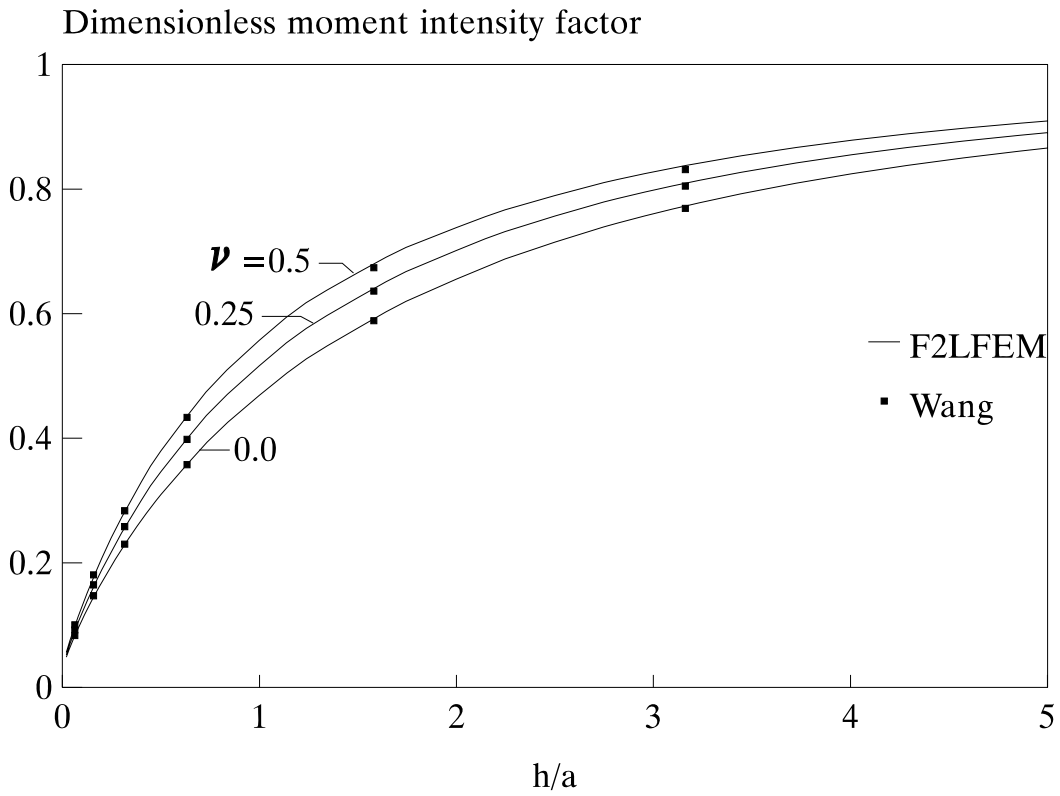

Figure 7. Variation of K2 versus ratio of plate thickness to crack length.

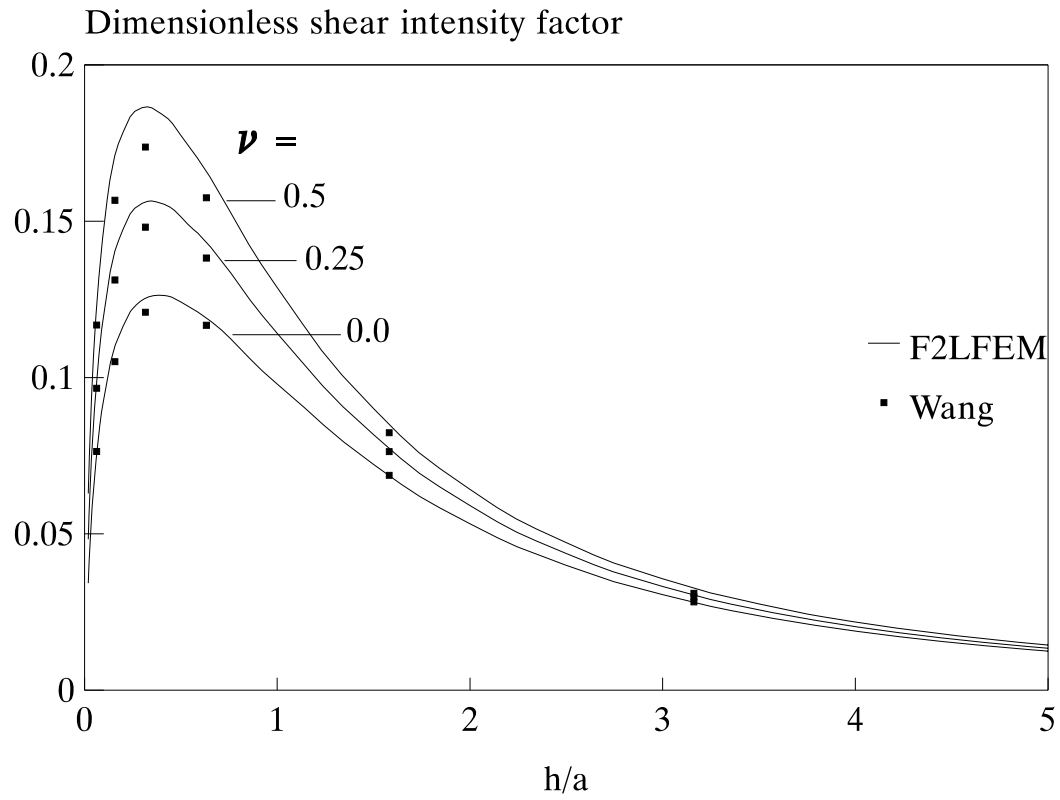

Figure 8. Variation of K3 versus ratio of plate thickness to crack length.